Opto-Electronics Review 29 (2021) 97-104

PAN POLISH ACADEMY OF SCIENCES

Opto-Electronics Review

journal homepage: http://journals.pan.pl/opelre

Solar cells based on copper oxide and titanium dioxide prepared by reactive direct-current magnetron sputtering

G. Wisz[a], P. Sawicka-Chudy[a], M. Sibiński[b], Z. Starowicz[c], D. Płoch[a], A. Góral[c], M. Bester[a], M. Cholewa[a], J. Woźny[b], A. Sosna-Głębska[b]

[a] Institute of Physics, College of Natural Sciences, University of Rzeszów, 1 Pigonia St., 35-310 Rzeszów, Poland
[b] Department of Semiconductor and Optoelectronic Devices, Łódź University of Technology, 211/215 Wólczańska St., 90-924 Łódź, Poland
[c] Institute of Metallurgy and Materials Science, Polish Academy of Sciences, 25 Reymonta St., 30-059 Kraków, Poland

Article info

Article history:
Received 22 Jun. 2021
Received in revised form 24 Sep. 2021
Accepted 25 Sep. 2021

Keywords:
solar cells,copper oxide,titanium dioxide,reactive magnetron sputtering

Abstract

In this study, solar cells based on copper oxide and titanium dioxide were successfully manufactured using the reactive direct-current magnetron sputtering (DC-MS) technique with similar process parameters. TiO_2/CuO, $TiO_2/Cu_2O/CuO/Cu_2O$, and TiO_2/Cu_2O solar cells were manufactured *via* this process. Values of short-circuit current efficiencies, short-circuit current density, open-circuit voltage, and maximum power of PV devices were investigated in the range of 0.02÷0.9%, 75÷350 μA, 75÷350 μA/cm^2, 16÷550 mV, and 0.6÷27 μW, respectively. The authors compare solar cells reaching the best and the worst conversion efficiency results. Thus, only the two selected solar cells were fully characterized using I-V characteristics, scanning electron microscopy, X-ray diffraction, ellipsometry, Hall effect measurements, and quantum efficiency. The best conversion efficiency of a solar cell presented in this work is about three times higher in comparison with the authors' previous PV devices.

1. Introduction

Traditional electricity/fossil fuel production contributes to acid rain, global warming, and environmental pollution. On the other hand, renewable energy sources (especially photovoltaic varieties) can have a positive impact on the environment to ultimately avoid global energy crises in the future [1,2]. The basic advantages of solar cells include: ability to obtain solar radiation energy, no negative impact on the environment, and long-term applicability and use. Currently, the most popular form of renewable energy sources are silicon solar cells. Thin-film solar cells are predestined to create a competitive, efficient, and cost-effective PV structure [3], as well as to replace traditional solar cells.

Copper oxide and titanium dioxide are promising materials for PV applications due to their non-toxic and cost-effective characteristics [4,5], copper and titanium natural abundance [4], easy and low-cost production methods, and environmentally friendly resources [6]. Thin-film solar cells based on copper oxide and titanium dioxide are attractive PV devices due to their versatile applications. Additionally, the theoretical limits of ideal solar cells are advantageous for solar cell applications which are 13.7% for TiO_2/Cu_2O, and 22.4% for TiO_2/CuO [7], or 28.6% for $TiO_2/CuO/Cu_2O$ and 16% for TiO_2/CuO for solar cells with defects [8].

In heterojunctions, based on copper oxide and titanium dioxide TiO_2 acts as a window layer and CuO (Cu_2O) is used as an absorption layer. A TiO_2 layer with a band gap of more than 3.0 eV [9] absorbs only ultraviolet solar light wavelengths (less than 8% of sunlight spectrum) [10] which is normally absorbed by the front encapsulation layer. Simultaneously, the properly matched and direct band gaps of copper oxides (from 2.0 to 2.5 eV for Cu_2O, and from 1.3 to 1.7 eV for CuO) [11] allow for the absorption of most of the solar spectrum due to the high value of the absorption coefficient [12]. Solar cells based on copper oxides and titanium dioxide have been studied extensively [4,5,9,10,12–15]. The best conversion efficiency has been achieved for TiO_2/CuO [6] equalling 1.62%.

*Corresponding author at: psawicka@ur.edu.pl

https://doi.org/10.24425/opelre.2021.139039.
1896-3757/ Association of Polish Electrical Engineers (SEP) and Polish Academic of Sciences (PAS). Published by PAS

In the earlier experiments, authors fabricated TiO_2/Cu_2O photovoltaic structures, but a PV effect was not observed [15]. After three years of the extensive research, TiO_2/CuO solar cells were successfully obtained with an efficiency of ~0.24% [16]. The results presented in this manuscript relate to new samples produced in different process conditions, which allowed for an increase of ~300% compared to previous works [16], e.g., by using a Cu buffer.

Currently, the efficiency of solar cells manufactured by the authors based on titanium and copper oxides increased to 0.9% because of modification of the process parameters which is reported below. The alternative cell configurations were manufactured and fully characterized.

2. Materials and methods

In this work, solar cells based on copper oxide and titanium dioxide, and single layers were fabricated by a reactive direct-current magnetron sputtering (DC-MS). Magnetron sputtering was selected as a promising process which could be used for a high-quality layer deposition onto larger areas [14]. The DC-MDX 1.5K power supply from Advanced Energy with ION'X planar magnetron sputtering cathode from Thin Film Consulting was used. Automatic limiting occurs when the current, voltage, or power exceeds set limits.

The investigated layers of copper oxide and titanium dioxide were produced with similar process parameters (Table 1), selected on the basis of the previous studies [15,16]. One TiO_2/CuO (#11), four $TiO_2/Cu_2O/CuO/Cu_2O$ (#12, #13, #14, #17), and TiO_2/Cu_2O (#16) solar cells were obtained.

A Ti target (99.995%) and a Cu target (99.995%) with 1 inch in diameter and ~6 mm in thickness were used, respectively. Targets were placed directly on the substrate in one axis, so that the surfaces were parallel to each other.

The solar cells were fabricated using the following method: a TiO_2 layer was deposited on indium-tin-oxide (ITO) coated glass, then a Cu buffer was used for 5 s in samples #12, #14, #16, #17, and for 10 s in sample #13 with 4 cm^3/s argon flow, and without oxygen flow. For sample #11, a Cu buffer was not used. A Cu layer between the titanium dioxide and the copper oxide was deposited to reduce the inter-layer stress.

Next, a CuO or Cu_2O thin film was deposited on the top of TiO_2 with a Cu buffer (Fig. 1). A Cu_2O thin film (in samples #12, #13, #14, #16, #17) was deposited using the same process guidelines (as with CuO), but there were other epitaxial conditions at the limiting substrate flow rate. For solar cells in $Cu_2O/CuO/Cu_2O$, a "Cu_2O layer" is formed at the beginning of the copper oxide layer until the flux relationship of the copper oxide substrate layer is stabilized and in the final stage when the beam of deposited species is destabilized.

Finally, a Cu thin film was deposited on the top of Cu_2O as a contact for few seconds on each sample (with no oxygen flow). To create a solar cell, Cu contacts were attached to the Cu and ITO using a conductive glue. The solar cell area was ~1 cm^2.

The upper Cu layer was added to improve the collection efficiency of the generated photocarriers, and in this case the efficiency of the whole PV structure.

The Cu layer was used in connection with the study of the possibility of limiting production costs of the target structures. According to literature reports, the best contact for this structure is gold [17], which, unfortunately, is very expensive and its use would limit the possibility of scaling and commercialization.

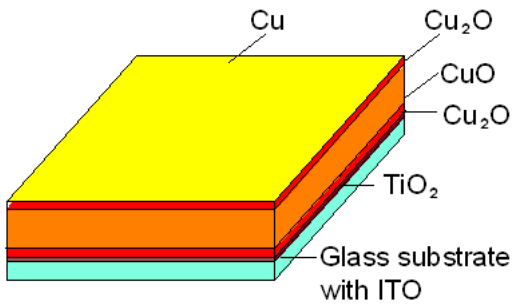

Fig. 1. Schematic structure of the $TiO_2/Cu_2O/CuO/Cu_2O/Cu$ solar cells.

Table 1.
The process parameters.

No.	Thin film	Cu buffer time [s]	Time [min]	Power [W]	Process preasure [Pa]	Distance between source and substrate [mm]	Oxygen flow rates [cm^3/s]	Argon flow rates [cm^3/s]	Substrate temperature [°C]
#11	TiO_2		20	120	1.0	58	3	0.5	200
	CuO	-	25	70	1.4	38	4	1	100
#12	TiO_2		23	120	1.1	58	4	0.5	300
	$Cu_2O/CuO/Cu_2O$	5	25	70	1.1	58	4	1	300
#13	TiO_2		25	120	1.1	58	4	0.5	300
	$Cu_2O/CuO/Cu_2O$	10	30	70	1.1	58	4	1	300
#14	TiO_2		25	120	1.2	58	4	0.5	300
	$Cu_2O/CuO/Cu_2O$	5	25	70	1.2	58	4	1	300
#16	TiO_2		20	120	0.7	58	2	0.5	300
	Cu_2O	5	25	70	3.1	58	4	4	350
#17	TiO_2		23	120	1.2	58	4	0.5	300
	$Cu_2O/CuO/Cu_2O$	5	35	70	1.2	58	4	1	300

The I-V characteristics of all solar cells were measured using a Keithley 2062 I-V meter and a halogen lamp as a light source with an intensity of ~500 W/m^2. Parameters of solar cells were measured under field conditions using a BM817s TRMS Brymen multimeter and the sun as a light source with an intensity of ~1000 W/m^2 controlled by a solar power meter APOGEE MP-200.

The scanning electron microscopy (SEM) image of thin-films heterojunctions was examined by a SEM Helios NanoLab 650 scanning electron microscopy. Ellipsometric measurements were made at incident angles of 50°, 60°, and 70° using a Sentech SE 800 PV Spectroscopic Ellipsometer at three random locations, and the results were averaged. A Bruker D8 Discover diffractometer with CoKα radiation was used to study phase compositions of the obtained solar cells. X-ray diffraction (XRD) patterns were measured by applying Bragg-Brentano (Θ-2Θ) geometry. The analysis of the phases was performed using a HighScore Plus and Diffrac.EVA software with an ICDD PDF-4+ crystallographic database. Electrical properties like resistivity, carrier concentration, and carrier mobility were obtained using the Van der Pauw technique [18], followed by Hall voltage VH measurements in the presence of a static magnetic field *B*. Next, the procedure described in the measurement as standard was followed [19]. For SEM images, ellipsometric measurements, XRD, and Hall voltage VH the samples were deposited on silicon.

The quantum efficiency of rectangular Van der Pauw geometry samples with four contacts located on the edges was measured, using a Bentham Instruments Limited PVE300 Photovoltaic EQE System. A dual tunable light source based on a xenon-quartz tungsten halogen dual source and single monochromators was used for measurements in the range of 250–1100 nm.

3. Results and discussion

3.1 I-V characteristics

The TiO_2/CuO (#11) solar cell achieved the lowest value of efficiency (0.021%). The sample was amorphous due to a significantly lower value of a substrate temperature (see Table 1.) Similar results were observed by Ziaja and Łowkis [20,21], thus, the TiO_2/CuO (#11) solar cell was not analysed in this work. Low value of efficiency was also obtained for sample #16 (~0.05%) due to the high value of argon flow rates (40%) which influenced a higher value of sputtering pressure. At a higher sputtering pressure (lower vacuum level) the quality of the sample was poorer [20,22].

The highest efficiency was achieved for sample #12 due to applicable time of deposition (23 min for TiO_2, and 25 min for Cu_2O/CuO/Cu_2O). Obtained I_{sc}, J_{sc}, V_{oc}, P, and η (efficiency) of solar cells are shown in Table 2.

The autors' best solar cell efficiency was higher than that reported by Hussain *et al.* [9], Ichimura *et al.* [13] and Sawicka-Chudy & Wisz *et al.* [16], but lower than that of Luo *et al.* [4], as well as Rokhmat [6].

Figure 2 shows the I-V characteristics for all solar cells. The linear I-V characteristics were invariably observed due to the high value of series resistance. I-V parameters of TiO_2/Cu_2O/CuO/Cu_2O solar cells are not sufficient for practical applications yet. The low value of V_{oc} due to the present defects was also observed by Hussain *et al.* [9,10], and the presence of Cu_2O phases at the top layers deteriorated the structure significantly. Nevertheless, clearly observed photovoltaic effects and some hints towards the improvement of R_s and R_{sh} values were achieved in subsequent experiments.

Table 2.
The results of solar cells based on copper oxide and titanium dioxide.

No.	Parameter				
	I_{sc} [μA]	J_{sc} [μA/cm^2]	V_{oc} [mV]	P_{max} [μW]	μ [%]
#11	75.0±0.6	75.0±1.1	25.0±0.2	0.6±0.1	0.021±0.004
#12	187.5±0.8	187.5±1.3	550.0±0.5	27±1	0.90±0.041
#13	162.5±0.7	162.5±1.3	300.0±0.4	13±1	0.433±0.032
#14	200.0±0.8	200.0±1.2	16.0±0.2	0.8±0.1	0.026±0.008
#16	350.0±1.1	350.0±1.3	25.0±0.2	1.5±0.1	0.050±0.012
#17	95.0±0.6	95.0±1.1	140.0±0.3	3.4±0.8	0.113±0.028

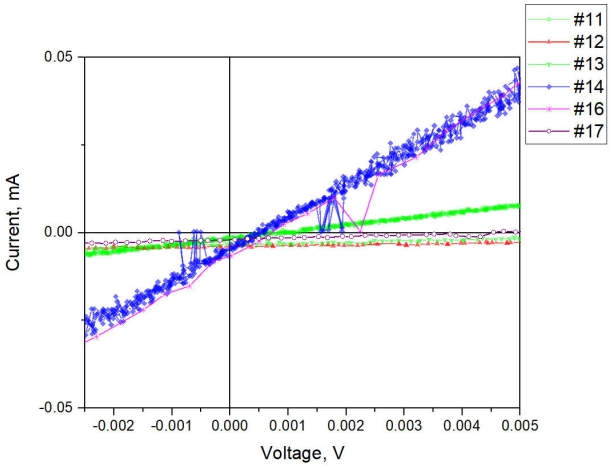

Fig. 2. I-V characteristics of all solar cells.

3.2 Structural characterization

The cross section and the surface morphology of a top SEM image of thin-films heterojunctions are shown in Figs. 3(a)-(d).

Sample #12 is significantly better than sample #16 due to the columnar homogeneous growth [Fig. 3(a)], and it is a separated phase boundary at the boundary of individual layers, unlike sample #16. The SEM image for #16 shows a very porous area which directly corresponds to the sample low yield.

In Fig. 3(a), clear interface structures are observed near the interface between CuO and TiO_2, and CuO and Cu_2O thin films. The cross section of TiO_2/Cu_2O/CuO/Cu_2O shows that the thicknesses of the TiO_2, Cu_2O, CuO, and Cu_2O layers were of 47 nm, 46 nm, 1200 nm, and 102 nm, respectively.

The above observations of the upper SEM image showed that the Cu layer is dense of various shapes particles with a size of around 160 nm–200 nm for sample #12. On the other hand, the observation of the upper SEM image showed that the grain was loose packed - with a size of around 300 nm–500 nm.

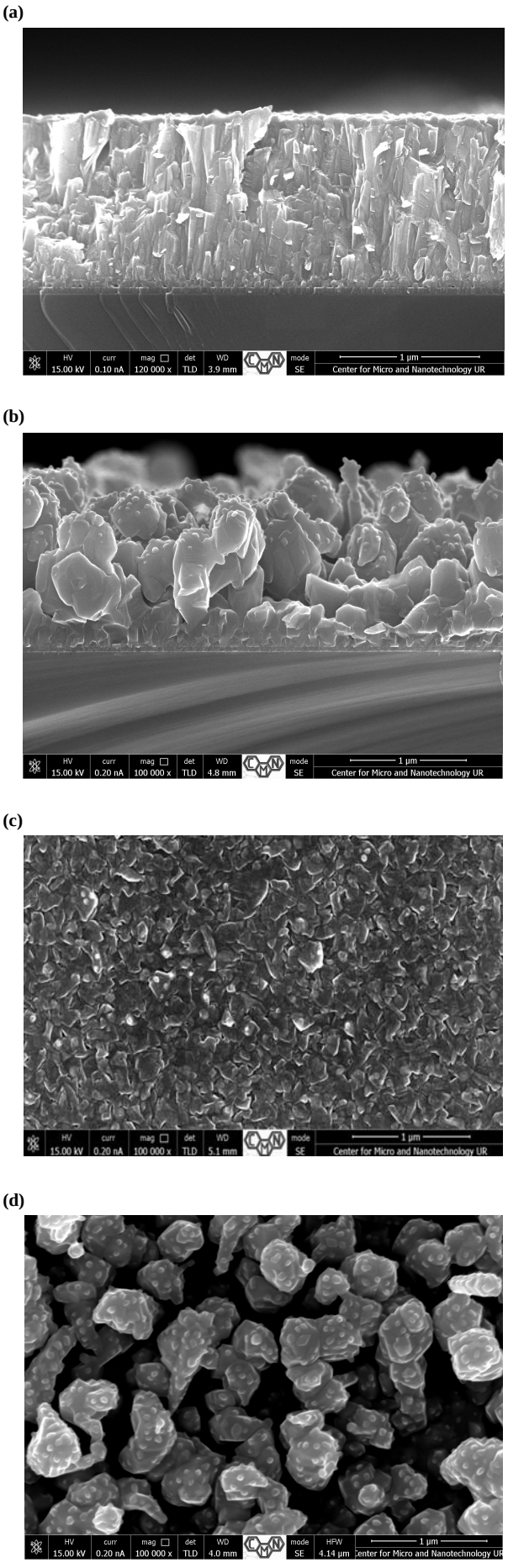

Fig. 3. The cross section of solar cells of #12 (a), #16 (b), and SEM microstructures of samples #12 (c) and #16 (d).

3.3 XRD study

The XRD patterns for $TiO_2/Cu_2O/CuO/Cu_2O$ and TiO_2/Cu_2O solar cells are shown in Figs. 4(a)-(b), respectively. XRD patterns show that the solar cells are composed of monoclinic CuO (C2/c), cubic Cu_2O (Pn-3m) phases for #12 and Cu_2O (Pn-3m), Cu (Fm-3m) for #16. Lattice parameters of the phases are presented in Table 3.

The XRD spectrum contained no peaks for TiO_2 due to the fact that the titanium oxide layer is very thin (~50 nm) and lies under thick copper oxide layers. The same observations have been reported by Hussain *et al.* [9]. For sample #12, the CuO and Cu_2O phases, peaks were

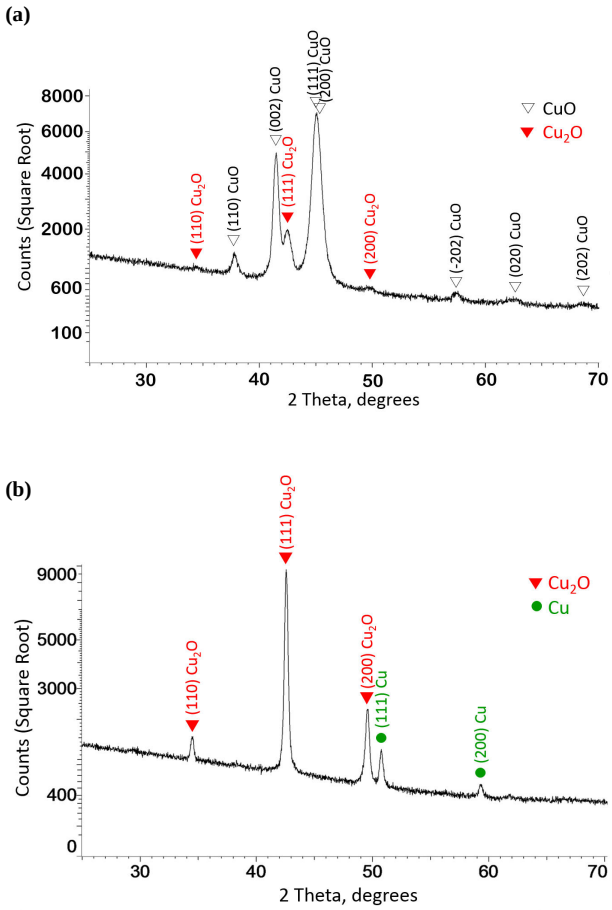

Fig. 4. X-ray diffraction pattern of samples: #12 (a) and #16 (b).

Table 3.
The phases identified in the obtained $TiO_2/Cu_2O/CuO/Cu_2O$ solar cells and theoretical lattice parameters.

Identified phases (space group)	Calculated lattice parameters	Theoretical lattice parameters
CuO (C2/c)	a [Å] = 4.660(5), b [Å] = 3.43(1), c [Å] = 5.13(2), α [°] = 90, β [°] = 98.82(8), γ [°] = 90	a [Å] = 4.6837, b [Å] = 3.4226, c [Å] = 5.1288, α [°] = 90, β [°] = 99.54°, γ [°] = 90 [23]
Cu_2O (Pn-3m)	a [Å] =4.265(8) (#12) a [Å] = 4.2705(3) (#16)	a [Å] = 4.2696 [24]
Cu (Fm-3m)	a [Å] = 3.6168(3)	a [Å] = 3.61491 [25]

observed at: (37.8º), (41.5º), (44.9º), (45.3º), (57.6º), (62.4º), (68.1º), and (34.4º), (42.5º), (49.4º), respectively [Fig. 4(a)]. Using Scherrer's equation [26], the crystallite sizes of CuO and Cu_2O were estimated and calculated from 41.5º (002) and 42.5º (111) diffraction peaks (crystallographic planes) and were equal to ~32 nm and 19 nm, respectively.

For sample #16, the Cu and Cu_2O phases, peaks were observed at: (34.5º), (42.5º), (49.5º), (72.7º), (88.1º), (93.1º), and (50.7º), (59.3º), respectively [Fig. 4(b)]. The crystallite sizes of Cu and Cu_2O were estimated and calculated from the diffraction peaks of 49.5º (200) and 50.7º (111) and were equal to 100 nm for Cu_2O and 140 nm for Cu. An almost five-fold increase in a crystallite size for Cu_2O has been observed due to higher argon flow rates for #16.

Theoretical lattice parameters were suitably calculated. Most probably, little differences are mainly due to their own material residual stress [27].

The mismatches of the CuO/Cu_2O lattice are given in the following equations for #12 [22]:

$$\frac{\Delta a}{a} = \frac{2(a_3 - a_1)}{a_3 + a_1} \quad \text{for } Cu_2O/TiO_2$$

$$\text{or} \quad \frac{\Delta a}{a} = \frac{2(a_2 - a_3)}{a_2 + a_3} \quad \text{for CuO/}Cu_2O, \qquad (1)$$

where a_1, a_2 and a_3 are the lattice constants of TiO_2, CuO, and Cu_2O, respectively, obtained from the XRD analysis. According to Eq. (1) ($a_1 = 3.804$ Å, $a_2 = 4.660$ Å, $a_3 = 4.265$ Å), the lattice mismatch between TiO_2 and Cu_2O equals ~11% which is more than two times lower than those reported by Hussain *et al*. for TiO_2/Cu_2O solar cells (~25%) [9] or reported by Zhang for ZnO/Cu_2O (~27%) [28]. The lattice mismatch between CuO and Cu_2O equals ~8.9%.

3.4 Optical properties

Ellipsometric measurements were made to determine the structure thicknesses and optical properties. The results of ellipsometric measurements for sample #12 are shown below.

For sample #16, analyses were not possible due to an excessively rough layer. Initially, the parameters of the TiO_2 layer were theoretically determined based on the separated samples.

Then, a copper oxide layer was determined by a Tauc-Lorentz multi-oscillator model. However, no proper fit could be found for the model of a single layer copper oxide. From the characteristics in the short wavelength range, it was concluded that two phases are contained and, possibly, Cu_2O is lying on the surface. The phase composition was consistent with the XRD findings. It can be associated with a thin layer distinguishable also in the SEM image just below the surface roughness. From this image, another layer standing out from the adjacent layer can be found at the interface of the Ti_2O and CuO absorber. The fitting procedure suggested existence of a complex structure which included Cu_2O on both sides of CuO. The optical model comprised the following structure: Si (100) substrate, 2.9-nm SiO_2 native oxide, 47 nm of TiO_2, followed by 46 nm of Cu_2O, 1089.2 nm of CuO covered with 48.1 nm of Cu_2O, finished with the surface roughness. In an ellipsometric model the surface roughness can be estimated as an effective balance of air to surface layer thickness, usually at a 50/50 ratio. In this structure, the thickness of the roughness layer was found to be of 15.7 nm which should be taken as an average, but areas of smaller or larger roughness are also possible. The mean square error of the simultaneous fitting of the 18 curves (Psi and Delta for 50, 60, and 70-degree incidence angles for three regions) equalled 6.5, confirming reasonable results. There was a very close correspondence of the obtained thickness of the copper oxide (1215 nm) SEM cross-section which ensured a reasonable assessment of the optical properties of individual layers. Figure 5 presents the optical constants of the refractive index and extinction coefficient for TiO_2, CuO, and Cu_2O.

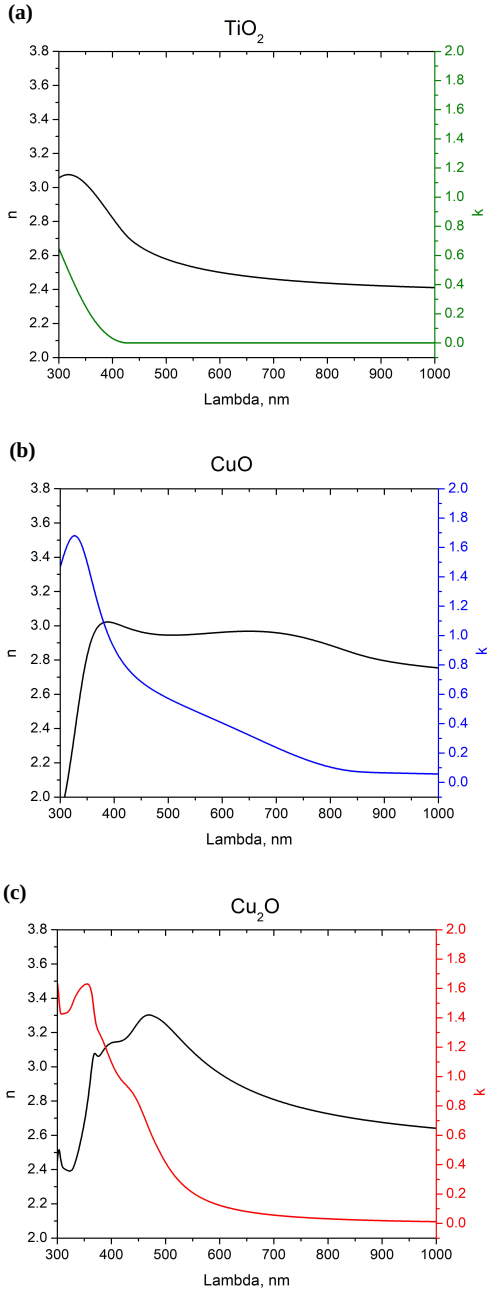

Fig. 5. Refractive index *n* and extinction coefficient *k* of deposited layers taken from ellipsometric fitting for sample #12 for TiO_2 layer (a), CuO layer (b), and Cu_2O layer (c).

Comparing two samples, the one with the high surface roughness should not be considered a solar cell absorber. Although the porous structure provides a very effective good light trapping, the larger surface area corresponds to numerous dangling bonds that are recombination centres, and, also, good electrical back contact seems unachievable.

3.5 *Active layers electrical properties/measurements*

To evaluate the mobility and carrier concentration, the sheet resistance R_{sh} must be initially calculated. This requires calculating resistances defined as the voltage between contacts on one side of the sample divided by currents flowing through other two contacts. Since there are four pairs of such contacts and two current directions can be used, eight resistances can be defined, see Ref. 15.

A standard rectangular sample with electrical contacts located at the edges of the sample has been used. The electrical contact between the active layer and the copper wiring was made using a silver conductive glue as is shown in Fig. 6.

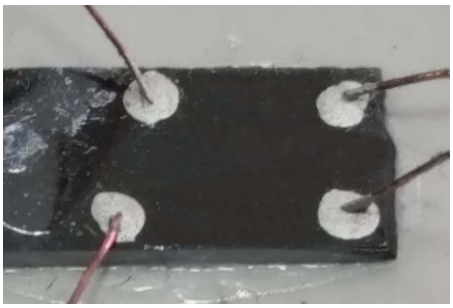

Fig. 6. Photo of one of the measured Van der Pauw geometry measured samples.

In this study, two layers of copper oxides (#12C, #16C) and two layers of titanium(IV) oxide (#12T, #16T) were measured. Unfortunately, the appropriate contact was achieved only for the copper oxide samples.

The I-V characteristics for each side pair of contacts is presented in Fig. 7.

Since the linearity of the contacts is not perfect and the was current from $-|I_{max}|$ to $+|I_{max}|$, the relevant resistances [Eq. (2)] are calculated as the ratio of the voltage gain to the current gain, not as the ratio of the absolute values [15].

$$R_{21,34}=\frac{\Delta V_{34}}{\Delta I_{21}} \quad R_{12,43}=\frac{\Delta V_{43}}{\Delta I_{12}}$$
$$R_{32,41}=\frac{\Delta V_{41}}{\Delta I_{32}} \quad R_{23,14}=\frac{\Delta V_{14}}{\Delta I_{23}} \qquad (2)$$
$$R_{43,12}=\frac{\Delta V_{12}}{\Delta I_{43}} \quad R_{34,21}=\frac{\Delta V_{21}}{\Delta I_{34}}$$
$$R_{14,23}=\frac{\Delta V_{23}}{\Delta I_{14}} \quad R_{41,32}=\frac{\Delta V_{32}}{\Delta I_{41}}$$

Hall effect measurement system was used to determine carrier mobility (μ), carrier concentration (n), and resistivity (ρ) which are shown in Table 4.

The range of mobility for CuO and CuO_2 thin films described in the existing literature is wide. The proposed mobility for most thin-layers carriers starts at 0.1 cm^2/Vs for CuO and reaches 100 cm^2/Vs for high Cu_2O mobility [29]. Overall, Hall mobility, measured horizontally, strongly depends on the size of nanocrystals. The grain boundaries limit the mobility of carriers in a horizontal direction. Thus, any process increasing the grain size improves the conductivity [30]. Most of CuO samples show a mobility of 1 up to 5 cm^2/Vs [30,31] at a concentration of 1015~1020 cm^{-3} which is in line with the values measured in this study.

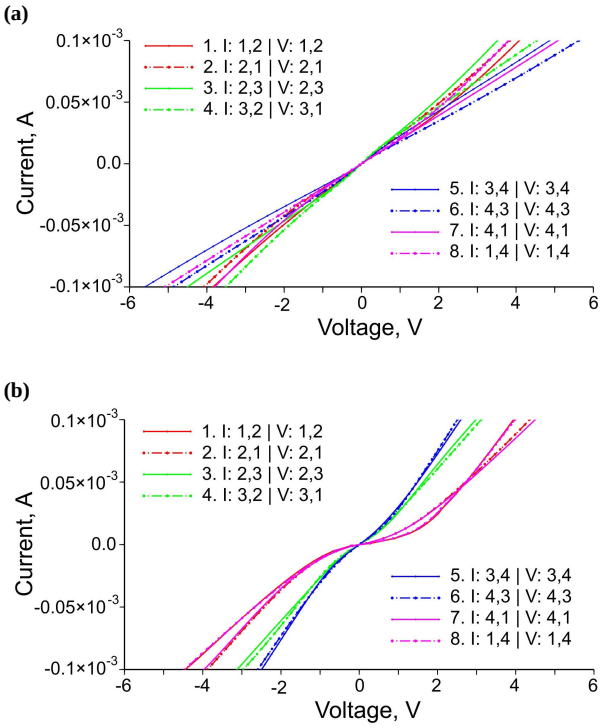

Fig. 7. The I-V characteristics for copper oxides sample #12 (a) and sample #16 (b).

Table 4.
Results of Hall effect measurement.

Sample	I_{max} [mA]	B [T]	ρ [Ωcm]	N [cm^{-3}]	μ [cm^2/Vs]
$\#12_C$	0.1	0.5	2.92	6×10^{17}	3.4
$\#16_C$	0.1	0.5	2.34	3×10^{17}	8.4

3.6 *Quantum efficiency*

Examples of external quantum efficiency (EQE) for #12 and #16 are shown in Fig. 8.

It can be clearly observed in Fig. 8 that the #12 solar cell is capable of absorbing and effectively converting visible light in the range of 300-500 nm, but the maximum quantum efficiency is only 8.5% at ~360 nm. A poor conversion at IR light is also observed above 750 nm. However, the local maximum is only 0.5% at 850 nm. In contrast, the maximum EQE peak of #16 is only 3% at ~350 nm and drops rapidly with a wavelength rise.

EQE characteristic of the sample #12 roughly covers the absorption range of Cu_2O with the absence of the CuO layer impact. This gives some positive feedback but confirms insufficient quality of the heterostructure operation and the base layer problems. However, the overall improper structure of sample #16 is fully reflected

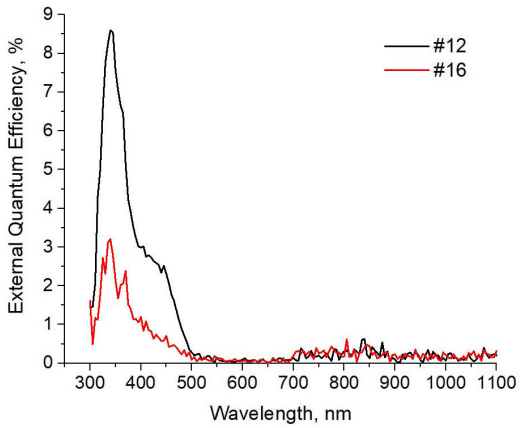

Fig. 8. External quantum efficiency for #12 and #16.

in the unsatisfactory flow of EQE characteristics. These parameters are key factors for the future high performance of the device and will, therefore, be the subject of further optimization.

4. Conclusions

To summarize, solar cells have been successfully manufactured by direct-current magnetron sputtering with the highest efficiency of 0.9% for #12 (with the following process parameters: substrate temperature during deposition of 300 °C and oxygen flow rate of 4 cm^3/s for Cu_2O/CuO and TiO_2, argon flow rate of 0.5 and 1 cm^3/s, time of deposition of 23 and 25 min for Cu_2O/CuO and TiO_2, respectively). The full structure of $TiO_2/Cu_2O/CuO/Cu_2O$ was obtained in a single processing mode, however, further optimization of the structure morphology is needed for a higher photogeneration effect.

Additionally, solar cells were characterized with I-V characteristics, scanning electron microscopy (SEM), X-ray diffraction (XRD), ellipsometric, Hall effect measurements, and quantum efficiency.

From above, the main conclusions of the work can be as follows:

- too low substrate temperature value while depositing thin films causes a low efficiency of 0.021% due to the amorphism of the layers,
- high value of argon flow rates (4 cm^3/s) resulted in a higher value of sputtering pressure and lower quality of samples – extensive roughness and voids,
- for $TiO_2/Cu_2O/CuO/Cu_2O$ solar cells, the low efficiency is mostly due to a large mismatch of CuO and Cu_2O lattice, Cu_2O phases, and the presence of defects and high series resistance. However, these parameters can be optimized by the process modification,
- EQE characteristics confirm the presence of a CuO layer as an absorber. Thus, the main influence of the high series resistance of solar cells is the CuO layer,
- heterostructure of $TiO_2/Cu_2O/CuO/Cu_2O$ (#12) seems to be the most attractive for effective copper-based thin-film cells commercialization from theoretical and technological point of view.

Appendix

The authors invite readers to watch a YouTube video of their work at the laboratory of University of Rzeszow, Poland by using the following links:
https://www.youtube.com/watch?v=-0Sn4UbiKaE
https://www.youtube.com/watch?v=Lavsm1CIqhY
https://www.youtube.com/watch?v=iei5bn2UAzg&t=35s
https://www.youtube.com/watch?v=0TjWJwxLZYk&t=4s

References

[1] Olczak, P., Kryzia, D., Matuszewska, D. & Kuta, M. "My Electricity" program effectiveness supporting the development of PV installation in Poland, *Energies* **14**, 231 (2021). https://doi.org/10.3390/en14010231

[2] Cader, J., Olczak, P. & Koneczna, R. Regional dependencies of interest in the 'My Electricity' photovoltaic subsidy program in Poland. *PolitykaEnergetyczna – Energy Policy Journal* **24**, 97–116 (2021). https://doi.org/10.33223/epj/133473

[3] Zhang, Y. & Park, N.-G. A thin film (<200 nm) perovskite solar cell with 18% efficiency. J. *Mater. Chem. A* **34** 17420–17428 (2020). https://doi.org/10.1039/D0TA05799A

[4] Luo, Y. *et al.* Electrochemically deposited Cu_2O on TiO_2 nanorod arrays for photovoltaic application. *Electrochem. Solid-State Lett.* **15**, H34–H36 (2012). https://doi.org/10.1149/2.016202esl

[5] Pavan, M. *et al.* TiO_2/Cu_2O all-oxide heterojunction solar cells produced by spray pyrolysis. *Sol. Energy Mater. Sol. Cells* **132**, 549–556 (2015). https://doi.org/10.1016/j.solmat.2014.10.005

[6] Rokhmat, M., Wibowo, E., Sutisna, Khairurrijal & Abdullah, M. Performance improvement of TiO_2/CuO solar cell by growing copper particle using fix current electroplating method. *Procedia Eng.* **170**, 72–77 (2017). https://doi.org/10.1016/j.proeng.2017.03.014

[7] Sawicka-Chudy, P. *et al.* Simulation of TiO_2/CuO solar cells with SCAPS-1D software. *Mater. Res. Express* **6**, 085918 (2019). https://doi.org/10.1088/2053-1591/ab22aa

[8] Zhu, L. Development of Metal Oxide Solar Cells through Numerical Modelling. (University of Bolton, Bolton, 2012).

[9] Hussain, S. *et al*. Fabrication and photovoltaic characteristics of Cu_2O/TiO_2 thin film heterojunction solar cell. *Thin Solid Films* **522**, 430–434 (2012). https://doi.org/10.1016/j.tsf.2012.08.013

[10] Hussain, S. *et al*. Cu_2O/TiO_2 nanoporous thin-film heterojunctions: Fabrication and electrical characterization. *Mater. Sci. Semicond. Process.* **25**, 181–185 (2014). https://doi.org/10.1016/j.mssp.2013.11.018

[11] Sawicka-Chudy, P. *et al.* Review of the development of copper oxides with titanium dioxide thin film solar cells. *AIP Adv.* **10**, 010701 (2020). https://doi.org/10.1063/1.5125433

[12] Yang, Y., Xu, D., Wu, Q. & Peng, D. Cu_2O/CuO bilayered composite as a high-efficiency photocathode for photoelectrochemical hydrogen evolution reaction. *Sci. Rep.* **6**, 35158 (2016). https://doi.org/10.1038/srep35158

[13] Ichimura, M. & Kato, Y. Fabrication of TiO_2/Cu_2O heterojunction solar cells by electrophoretic deposition and electrodeposition. *Mater. Sci. Semicond. Process.* **16**, 1538–1541 (2013). https://doi.org/10.1016/j.mssp.2013.05.004

[14] Zhang, W., Li, Y., Zhu, S. & Wang, F. Influence of argon flow rate on TiO_2 photocatalyst film deposited by dc reactive magnetron sputtering. *Surf. Coat. Technol.* **182**, 192–198 (2004). https://doi.org/10.1016/j.surfcoat.2003.08.050

[15] Sawicka-Chudy, P. *et al.* Characteristics of TiO_2, Cu_2O, and TiO_2/Cu_2O thin films for application in PV devices. *AIP Adv.* **9**, 055206 (2019). https://doi.org/10.1063/1.5093037

[16] Sawicka-Chudy, P. *et al*. Performance improvement of TiO_2/CuO by increasing oxygen flow rates and substrate temperature using DC reactive magnetron sputtering method. *Optik* **206**, 164297 (2020). https://doi.org/10.1016/j.ijleo.2020.164297

[17] Li, D. *et al*. Prototype of a scalable core–shell Cu_2O/TiO_2 solar cell. *Chem. Phys. Lett.* **501**, 446–450 (2011). http://doi.org/10.1016/j.cplett.2010.11.064

[18] van der Pauw, L. J. A method of measuring specific resistivity and Hall effect of discs of arbitrary shape. *Philips Res. Rep.* **13**, 1–9 (1958). https://doi.org/10.1142/9789814503464_0017

[19] ASTM F76-08(2016)e1, Standard Test Methods for Measuring Resistivity and Hall Coefficient and Determining Hall Mobility in, Single-Crystal Semiconductors (ASTM International, West Conshohocken, USA, 2016). https://doi.org/10.1520/F0076-08R16E01

[20] Ziaja, J. *Cienkowarstwowe Struktury Metaliczne i Tlenkowe. Właściwości, Technologia, Zastosowanie w Elektrotechnice* (Oficyna Wydawnicza Politechniki Wrocławskiej, Wrocław, 2012). [in Polish]

[21] Łowkis, B., Ziaja, J., Klaus P. & Krawczyk D. Effect of magnetron sputtering parameters on dielectric properties of PTFE foil. *IEEE Trans. Dielectr. Electr. Insul.* **27**, 837–841 (2020). https://doi.org/10.1109/TDEI.2020.008710

[22] Gulkowski, S. & Krawczak, E. RF/DC magnetron sputtering deposition of thin layers for solar cell fabrication. *Coatings* **10**, 1–14 (2020). https://doi.org/10.3390/coatings10080791

[23] Forsyth J.B, Hull S. The effect of hydrostatic pressure on the ambient temperature structure of CuO. J. Phys.: Condens. Matter **3**, 5257-5261 (1991). https://doi.org/10.1088/0953-8984/3/28/001

[24] Hanke, L., Fröhlich, D., Ivanov, A., Littlewood, P. B. & Stolz, H. LA Phonoritons in Cu_2O. *Phys. Rev. Lett.* **83**, 4365–4368 (1999). https://doi.org/10.1103/PhysRevLett.83.4365

[25] Straumanis, M. E. & Yu, L. S. Lattice parameters, densities, expansion coefficients and perfection of structure of Cu and Cu-In alpha phase. *Acta Cryst.* **A25**, 676–682 (1969). https://doi.org/10.1107/S0567739469001549

[26] Scherrer, P. Bestimmung der inneren Struktur und der Größe von Kolloidteilchen mittels Röntgenstrahlen. in *Kolloidchemie Ein Lehrbuch* 387–409 (Springer Berlin, Heidelberg, 1912). https://doi.org/10.1007/978-3-662-33915-2_7

[27] Chrzanowska-Giżyńska, J. Cienkie warstwy z borków wolframu osadzane impulsem laserowym i metodą rozpylania magnetronowego –wpływ parametrów procesu na osadzone warstwy. (Instytut Podstawowych Problemów Techniki, Polska Akademia Nauk, Warszawa, 2017). [in Polish]

[28] Zhang, D. K., Liu, Y. C., Liu, Y. L. & Yang, H. The electrical properties and the interfaces of Cu_2O/ZnO/ITO p–i–n heterojunction. *Physica B* **351**, 178–183 (2004). https://doi.org/10.1016/j.physb.2004.06.003

[29] Wong, T. K., Zhuk, S., Masudy-Panah, S. & Dalapati, G. K. Current status and future prospects of copper oxide heterojunction solar cells. *Materials* **9**, 271 (2016). https://doi.org/10.3390/ma9040271

[30] Gao, X., Du, Y. & Meng, X. Cupric oxide film with a record hole mobility of 48.44 cm^2/Vs via direct–current reactive magnetron sputtering for perovskite solar cell application. *Sol. Energy* **191**, 205–209 (2019). https://doi.org/10.1016/j.solener.2019.08.080

[31] Hu, X. *et al.* Influence of oxygen pressure on the structural and electrical properties of CuO thin films prepared by pulsed laser deposition. *Mater. Lett.* **176**, 282–284 (2016). https://doi.org/10.1016/j.matlet.2016.04.055